Available online at www.sciencedirect.com
SCIENCE DIRECT®

Journal of the European Ceramic Society 23 (2003) 2211–2223

www.elsevier.com/locate/jeurceramsoc

Characterisation of early stage calcium aluminate cement hydration by combination of non-destructive techniques: acoustic emission and X-ray tomography

T.J. Chotard[a,b,*], A. Smith[a], M.P. Boncoeur[c], D. Fargeot[a,b], C. Gault[a]

[a]*Groupe d'Etude des Matériaux Hétérogènes (GEMH, EA 3178) Ecole Nationale Supérieure de Céramique Industrielle, 47 à 73 Avenue Albert Thomas, 87065 Limoges Cedex, France*

[b]*Institut Universitaire de Technologie, Département Génie Mécanique et Productique, 2 allée André Maurois, 87065 Limoges Cedex, France*

[c]*Département de Radiologie, Centre Hospitalier Universitaire DUPUYTREN, 2, avenue Martin Luther King, 87042 Limoges Cedex, France*

Received 26 July 2002; received in revised form 17 January 2003; accepted 24 January 2003

Abstract

Techniques that monitor in real time the setting and hardening of calcium aluminate cements (CAC) are now of interest to the engineering community. This paper focuses on the association of two in situ techniques, acoustic emission (AE) and X-rays computed tomography (CT). These non-destructive techniques make it possible to follow the cement hydration in the early stage from a few minutes to a few hours after mixing. Results concerning a calcium aluminate cement paste, Secar71, are presented (water to cement weight ratio: 0.33; duration: 0–24 h). Both the acoustic emission (AE) signals and X-rays absorption values were recorded and analysed. Information deduced from experiments clearly show that a close correlation exists between the variations of the X-ray absorption values and the AE activity during the early stage of hydration. Based on the experiments, the combined analysis (quantitative and qualitative) of both AE and CT data make it possible to propose a relationship between the experimental characteristics recorded during the tests and the different mechanisms taking place during the early hydration of a cement paste. A chronology of cement setting is also proposed.

Keywords: Acoustic emission; Calcium aluminate cement; Cements; Hydration; X-ray tomography

1. Introduction

Calcium aluminate cements (CACs) are the only cements other than Portland cement in continuous, long-term production. Their success comes from their ability to withstand aggressive environments. They are a range of ceramic materials which are of interest not only to industrialists for a substantial market in civil engineering, in the refractory industry or in specific niches, but also to the materials science community.[1–3] Since the final characteristics of the set product are closely related to the first stage behaviour—i.e. from a few minutes to a few hours after the mixing of the constituents, different studies reported in the literature are concerned with the description of the nature and the formation of hydrates during this early stage.[4–9] Up to now, different types of experimental technique have been investigated to characterise the hydration of these pastes. They can be divided into two main categories: ex situ techniques (X-rays diffraction, differential thermal analysis, thermogravimetric measurements), and in situ methods such as proton and aluminium nuclear magnetic resonance,[10] neutron diffraction,[11,12] or ultrasonic measurements.[13–21] One interest with ultrasonic techniques is the possibility to evaluate the mechanical characteristics of the sample under test. Generally speaking, there is a need for characterisation techniques capable of providing information on large samples rather than small ones. In the present paper, we show the application of two in situ and non-destructive techniques, namely acoustic emission (AE) and X-rays computed tomography (CT), to follow the early stage hydration of

* Corresponding author.
E-mail addresses: t.chotard@ensci.fr (T.J. Chotard), a.smith@ensci.fe (A. Smith).

0955-2219/03/$ - see front matter © 2003 Elsevier Ltd. All rights reserved.
doi:10.1016/S0955-2219(03)00082-7

a CAC paste. These two techniques have already proven their reliability to characterise changes such as damage growth, density gradient, and so on in many types of materials and applications.[22–26]

2. Experimental procedure

2.1. Preparation of the cement paste

Although it is well known that CACs are used in very low amounts in commercial products such as refractory castables, it was decided to use a large sample of paste alone in order to focus the study on the hydration reaction of the cement. CAC has its own reactivity and mixing it with other constituents (sands, admixtures or other mineral charges) can modify the kinetics of the hydration reaction due to the possible interaction between the cement and the other products. The results presented in this paper refer to an aluminous material (Secar71) manufactured by Lafarge Aluminate and stored for a short period. This precaution is necessary to avoid any alteration of the cement grains by adsorption of water or carbon dioxide. The particle size distribution ranges between 0.3 and 100 μm with an average size around 10 μm. Its composition and physical characteristics are given in Table 1.

One lot of paste was prepared with a water-to-cement weight ratio (W/C) equal to 0.33. This lot was mixed according to the normalised procedure NF EN 196-3 (August 1995). Before mixing, the constituents were kept at the mixing temperature for 12 h. After mixing, the paste was poured into a silicone foam mould (90 mm×90 mm×30 mm) prior to the AE and CT measurements. The dimensions of the mould were chosen to be representative of the behaviour of large volumes of material. Silicone foam was selected as a mould material in view of its ability to deform in order to follow the shrinkage of the cement paste during hydration. The possibility of separation between the mould and the cement was then reduced and the related parasite noises were avoided. For this lot, at least three AE characterisations were carried out to check the reproducibility of the data. The experiments have been carried out at 20 °C and 95% relative humidity.

Table 1
Chemical composition, either in nature of cementitous phase or in oxide, for the cement

Chemical composition		Percentage (wt.%)
Cementitous phase	$CaAl_2O_4$ (or CA)	56
	$CaAl_4O_7$ (or CA)	38
	$Al_2O_3\alpha$	<6
	$Ca_{12}Al_{14}O_{33}$ (or $C_{12}A_7$)	<1
Oxide	CaO	26.6–29.2 wt.%
	Al_2O_3	69.8–72.2 wt.%

2.2. Background on CACs hydration process

The description of hydration mechanisms in aluminous cements is based on congruent dissolution of anhydrous phases followed by precipitation of hydrates.[27] Experiments on diluted systems were interpreted using this approach. Grains of CA dissolve to yield the species of Ca^{2+} and $Al(OH)_4^-$. Their concentration rapidly reaches supersaturation for hydrates formation. Therefore, germs of hydrates start to nucleate. After this nucleation, the so-called ''dormant period'', the germs grow until they reach a critical size. Thereafter there is a massive precipitation of hydrates, which is accompanied by substantial heat generation. In reality, even if the germs start growing very early, i.e. just after the mixing of the constituents, they cannot be detected immediately by experimental techniques such as thermal analysis, scanning electron microscopy (SEM) or X-ray diffraction. In this last case, if crystalline, the germs of the formed hydrates are too small to be detected; alternatively, if the germs are in their amorphous form, the problem is accentuated.

In the case of CAC, the type of hydrates formed is temperature dependent. Four different types of hydrates can be present in the material, namely CAH_{10}, C_2AH_8, C_3AH_6 and AH_3 in cementitous notation (C for CaO, A for Al_2O_3 and H for H_2O), according to the following reactions:

$$CA + 10H \rightarrow CAH_{10} \quad T < 15°C \tag{1}$$

$$2CA + 11H \rightarrow C_2AH_8 + AH_3 \quad 15°C < T < 30°C \tag{2}$$

$$3CA + 12H \rightarrow C_3AH_6 + 2AH_3 \quad T > 30°C \tag{3}$$

In practice, the mentioned temperature limits are not strict and the different hydrates can co-exist together.

2.3. Characterisation techniques

2.3.1. Acoustic emission

The acoustic emission (AE) technique is a well-known non-destructive evaluation technique to monitor flaw formation and failures in structural materials. It has been used on both the laboratory level and the industrial scale. Moreover, this method has been developed to characterise numerous structural components, such as steam pipes and pressure vessels, and in the research areas of rocks, composite materials, and metals. Acoustic emission is defined as ''the class of phenomena

whereby transient elastic waves are generated by the rapid release of energy from localised sources within a material (or structure); it also refers to the transient waves so generated''. It is mainly used to monitor the onset of cracking processes in materials and components essentially submitted to external loading. When a material is submitted to stresses, acoustic emission can be generated by a variety of sources, including crack nucleation and propagation, multiple dislocation slip, twinning, grain boundary sliding, Barkhausen effect (realignment or growth of magnetic domains), phase transformations in alloys, debonding of fibres in composite materials or fracture of inclusions in alloys.[28–31] In the case of hard concrete structures submitted to mechanical loading, AE events occur when cracks develop in the concrete and stress waves are emitted.[32,33] One of AE's great advantages is its ability to scan a large structure with only a few sensors and to localise the source causing the captured AE transient. In the present work, we propose a new use of AE. The technique will be used to record the elastic waves emitted during the chemical reactions and physical changes that occur during the hydration of the cement paste. The specificity here is two fold:

(i) characterisation is done on a paste as it transforms into a solid,
(ii) no external load is applied on the system under study.

The AE experimental set-up consists of an AEDSP-32/16 MISTRAS digital system from Physical Acoustics Corporation. This system makes it possible to record the waveform and the main AE parameters such as count, hit, rise time, duration of hit, count to peak and amplitude (in dB). Fig. 1 presents the different AE features extracted from the signal waveform.

Two sensors (PAC MICROPHONE R15), one test sensor and one reference sensor, with a bandwidth from 50 to 250 kHz, are connected through preamplifiers (EPA 1220A). The reference sensor is used in order to record noises due to the electromagnetic environment so that these parasite signals can be eventually subtracted from the ones recorded on the test sensor. A coupling fluid (Dough 428 Rhodorsil Silicone) is used to have an airless and flawless contact between the transducer and the specimen. The AE experimental set-up used in this work is presented in Fig. 2.

2.3.2. X-ray tomography

X-ray computed tomography was used to describe density changes in the material during hydration from a few minutes to a few hours after mixing. This technique allows the transmittance, T, through distance d of the sample under test to be measured. T is defined by the Beer–Lambert law:

$$T = \frac{I}{I_0} = e^{-(\mu d)} \tag{4}$$

where I and I_0 are the final and the initial intensities, respectively. μ corresponds to the linear absorption coefficient (in cm^{-1}); it depends on the wavelength of the radiation, the nature of the absorber and is directly related to the atomic density in the material.[34]

Eq. (4) only applies to monochromatic X-rays and to a perfectly homogeneous material. A typical medical system uses a source that emits polychromatic electromagnetic waves. The used CT system is assumed, however, with its continued area of beam, to operate on volume elements which are small enough to be considered homogeneous. As the absorption (also called attenuation = 1−transmittance), can be easily deduced from Eq. (4), the collection of absorption measurements

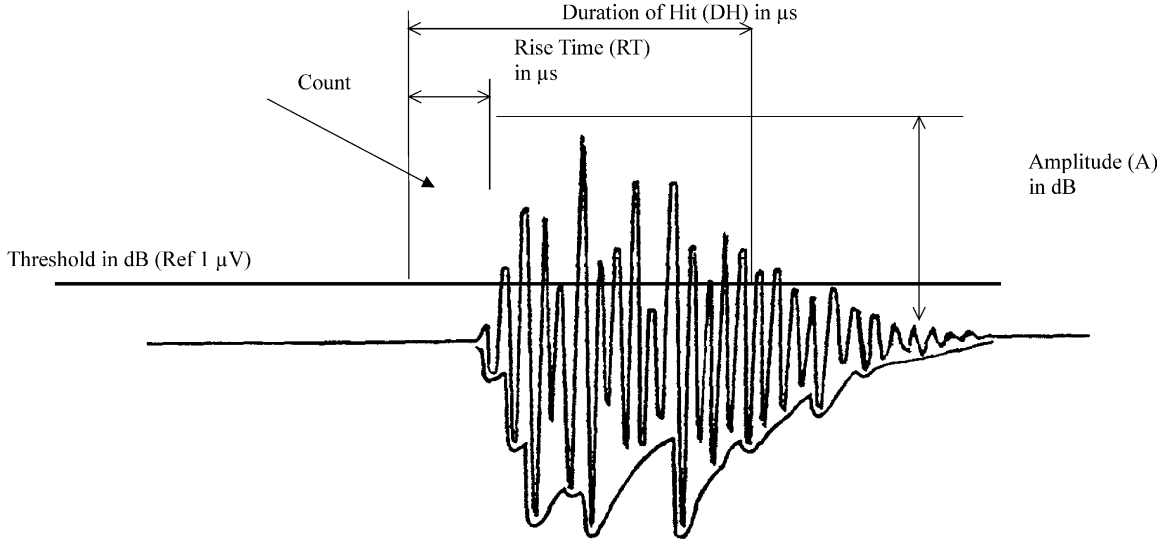

Fig. 1. Typical AE signal recorded with its associated characteristics.

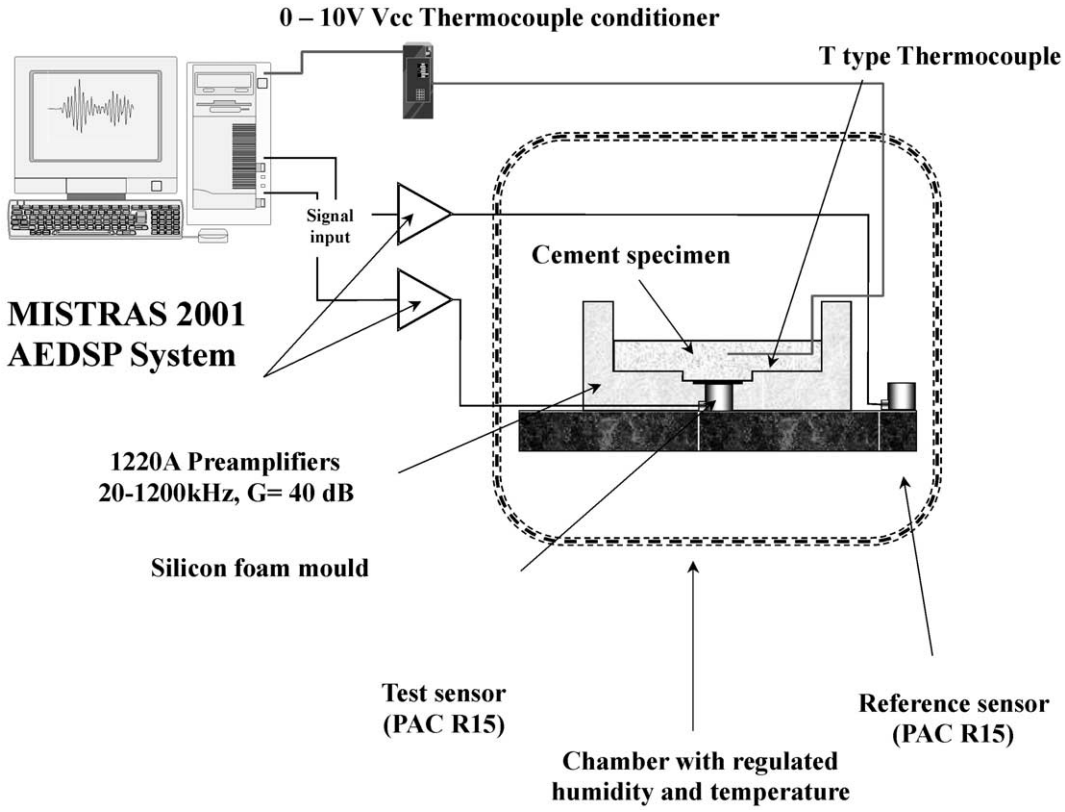

Fig. 2. Experimental set-up used for AE measurements.

over many limited area views allows a 2-D cross sectional image (CT image) to be mathematically reconstructed. The values of the absorption coefficients are transformed into CT numbers using the international Hounsfield scale:

$$\text{CT number} = \frac{\mu_{\text{material}} - \mu_{\text{water}}}{\mu_{\text{water}}} \times 1000(\text{HU}) \quad (5)$$

where μ_{material} and μ_{water} are the linear absorption coefficients (in cm^{-1}) of the material under test and water, respectively. The CT numbers, in Hounsfield units (HU), are representative of the mean X-rays absorption associated with each element area of the CT image. The result of this computer treatment is a map of linear absorption coefficients within the studied cross-section. Table 2 gives the CT scan parameters of the equipment (model high Speed Advantage from GE Inc.).

In order to describe the absorption variations as a function of setting time at either a bulk or local scale, 2D reconstructions of the sample were done from slices 1 mm thick. These slices were contiguous. Considering the initial dimensions of the sample, 90 views were taken in order to scan the whole specimen. For three selected slices (two towards the sample edges, one in the middle), different types of CT measurements were carried out; the scanning configuration is shown in Fig. 3. On each slice, the variations of CT number along longitudinal (y) and vertical (z) lines were taken (line graph). In addition, the average values of CT number for special regions of interest of the slice (ROI) were also taken. Finally, a histogram of the CT images (CT numbers distribution) was recorded. Fig. 4 illustrates these different measurements.

3. Results and discussion

3.1. Acoustic emission

Fig. 5 shows the variations of the number of AE cumulative hits and the temperature as a function of

Table 2
CT scan standard parameters

Parameter	Standard setting
Field of view (FOV)	150 mm
Slice thickness	1 mm/5 mm
Type of slice	Contiguous
Slice per sample	90/20
Display matrix	512×512 pixels
Reconstruction matrix	512×512 pixels
Spatial resolution	(150/512)≈300 μm
Exposure time	1 s
X-ray tube voltage	120 kV
X-ray tube current	200 mA

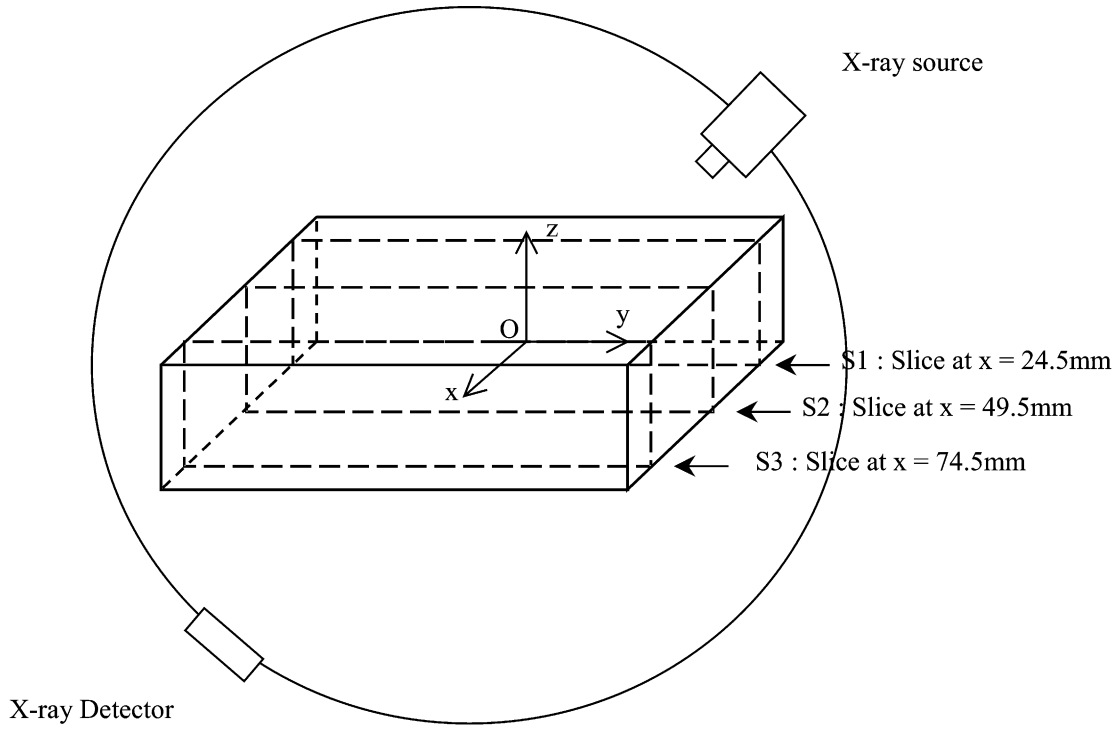

Fig. 3. X-rays computed tomography scanning configuration of the cement specimen.

time after mixing for the cement contained in the silicon foam mould. From these data, different characteristics (times and rates) have been graphically determined as shown in Fig. 6. t_T^{Start} and $t_{\mathrm{AE}}^{\mathrm{Start}}$ refer to the times when there is a significant modification of slope for T and the number of cumulative hits, respectively. t_T^{Infl} and t_T^{Max} correspond to the times when a notable change in temperature rate is observed and when the internal temperature reaches its maximum value, respectively. $\frac{\partial T}{\partial t}$ is the rate of increase of the internal temperature. We deliberately do not discuss the decrease of the internal temperature due to the role of the thermal coefficient (diffusion) of the silicon foam mould. Table 3 reports the different values taken by these characteristic times.

From data in Table 3 and Fig. 5, we observe that a large exothermic phenomenon starts earlier than the AE activity (AE cumulative hits) since $t_T^{\mathrm{Start}} < t_{\mathrm{AE}}^{\mathrm{Start}}$. Another point concerns the variation of temperature. A significant change in the temperature rate occurs at $t_T^{\mathrm{Infl}} = 3.07$ h until the time when the temperature reaches its maximum value ($t_T^{\mathrm{Max}} = 3.70$ h, $T = 48.1$ °C). As the internal temperature measured in a cement specimen is commonly used as a marker of hydration reaction, we can assume that before t_T^{Start}, the cement is in its dormant period where the anhydrous phase dissolves and a small amount of hydrates starts to nucleate. It should be remembered that this small amount of hydrates cannot be detected during this stage by conventional ex-situ techniques such as X-ray diffraction (XRD) or Differential Thermal Analysis (DTA).[27] At t_T^{Start}, we observe a notable rise of the internal temperature which corresponds to the beginning of hydrates precipitation ($\frac{\partial T}{\partial t} = 13$ °C/h). As this reaction goes on, we notice a significant change in the temperature rate ($\frac{\partial T}{\partial t} = 24$ °C/h). This could be correlated to a massive precipitation of hydrates.

In order to correlate the AE activity with the internal temperature measurements, Fig. 7 presents a magnification of Fig. 5 for the first 12 h. From this figure, six different AE periods can be distinguished. In Fig. 8, we have plotted the number of AE cumulative counts versus the number of AE cumulative hits. We notice that this plot also divides into six regions; each lasts for a duration which corresponds to what is reported on Fig. 7. The interest in plotting the cumulative counts versus cumulative hits is double. Firstly, the number of hits is known to be representative of the acoustic activity of a phenomenon; secondly, the number of counts can be associated to the global energy released by the same phenomenon. In fact, as already mentioned in the literature,[35] for the same AE activity (hit), the higher the emitted energy is, the higher the amplitude and the longer its duration are, and consequently the larger is the number of counts. This hypothesis is fulfilled in our case as shown in Fig. 9. This figure shows that the higher the amplitude and duration values are, the higher the number of recorded counts is. Therefore, in the case of cement hydration, we can say that six stages take place; amongst the active phenomena, we can quote growth of crystalline phases, friction between hydrates during tangling, emptying of capillary pores, microcracking due to stress relaxation during shrinkage and

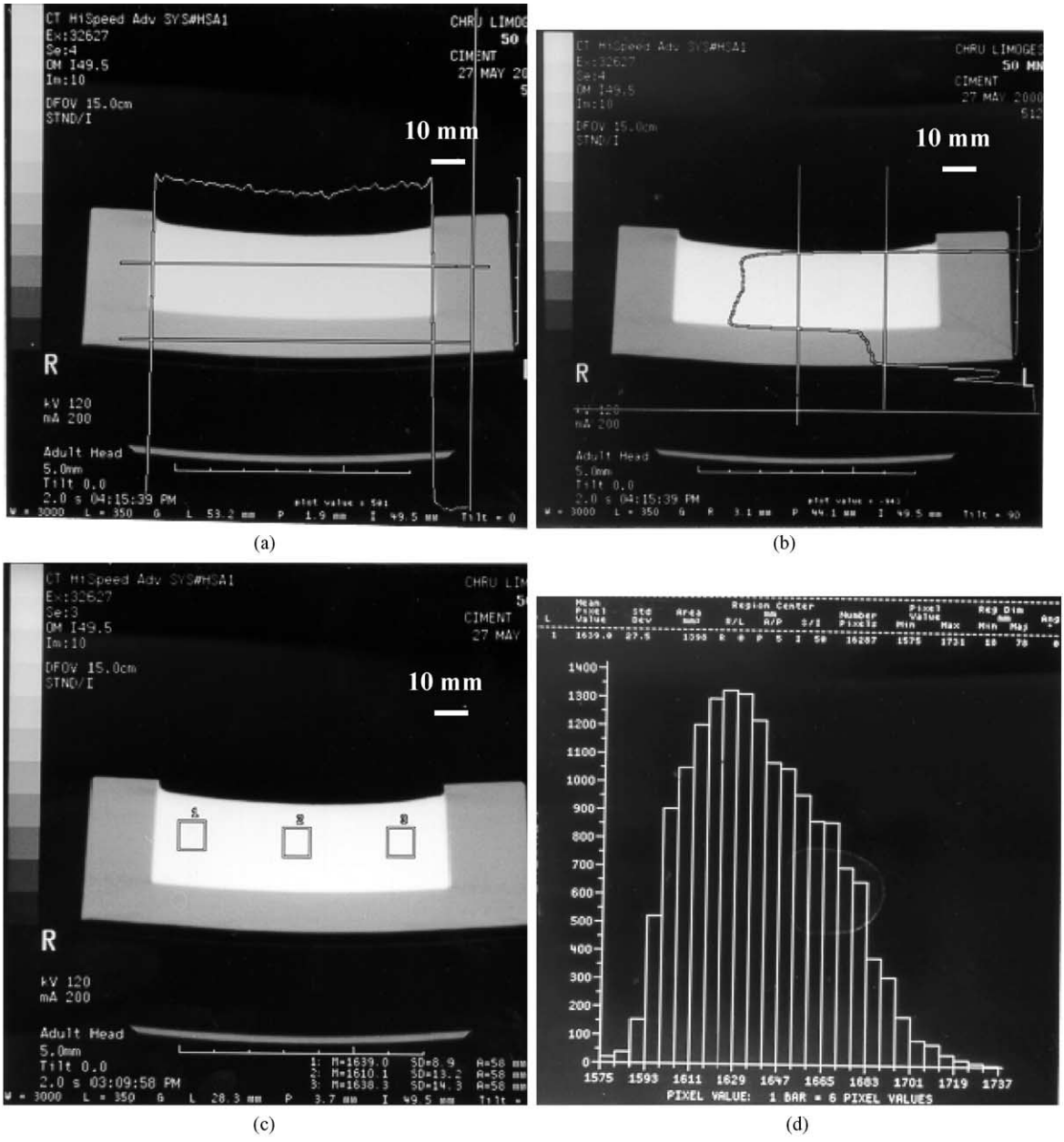

Fig. 4. Examples of typical CT measurements: (a) Longitudinal line graph, (b) Vertical line graph, (c) R.O.I. (1: left, 2: centre, 3: right), (d) histogram.

so on. Table 4 summarises the results. It should be noted that during the first 2.67 h, no acoustic emission has been recorded. If we compare AE feature with the internal temperature evolution for this period, we have noticed that $t_T^{\text{Start}} < t_{\text{AE}}^{\text{Start}}$. This experimental fact can lead to two hypotheses concerning the AE technique:

(i) the energy generated by the dissolution of the anhydrous phase or the nucleation of hydrates is too low to be detected by the AE technique;
(ii) the dissolution of the anhydrous phase or the nucleation of hydrates does not generate any acoustic activity.

Experimental evidence for these two hypotheses, carried out on model systems, is currently being obtained.

During the first and the second periods [(I): 2.67–2.81 h, (II): 2.81–3.19 h], the AE activity slightly increases with a value of the hit rate reaching 57.1 and 60.5 h^{-1}, respectively. In the same time intervals, the value of the average number of counts per hit remains relatively low, 4.1 and 5.1, respectively. Nevertheless, a slight variation of this parameter can be characteristic of a change in the hydration reaction. In fact, if we look simultaneously at the temperature evolution (i.e. Fig. 7), we note an inflexion in the curve at $t_T^{\text{Infl}} = 3.07$ h which can mark the

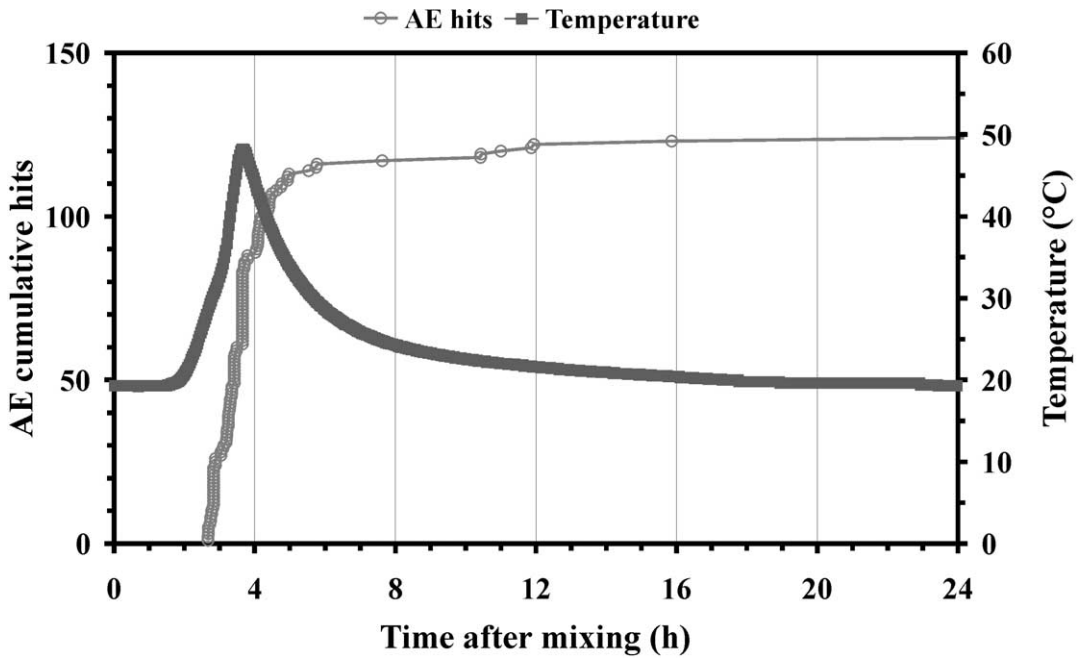

Fig. 5. AE cumulative number of hits and internal temperature as a function of time after mixing.

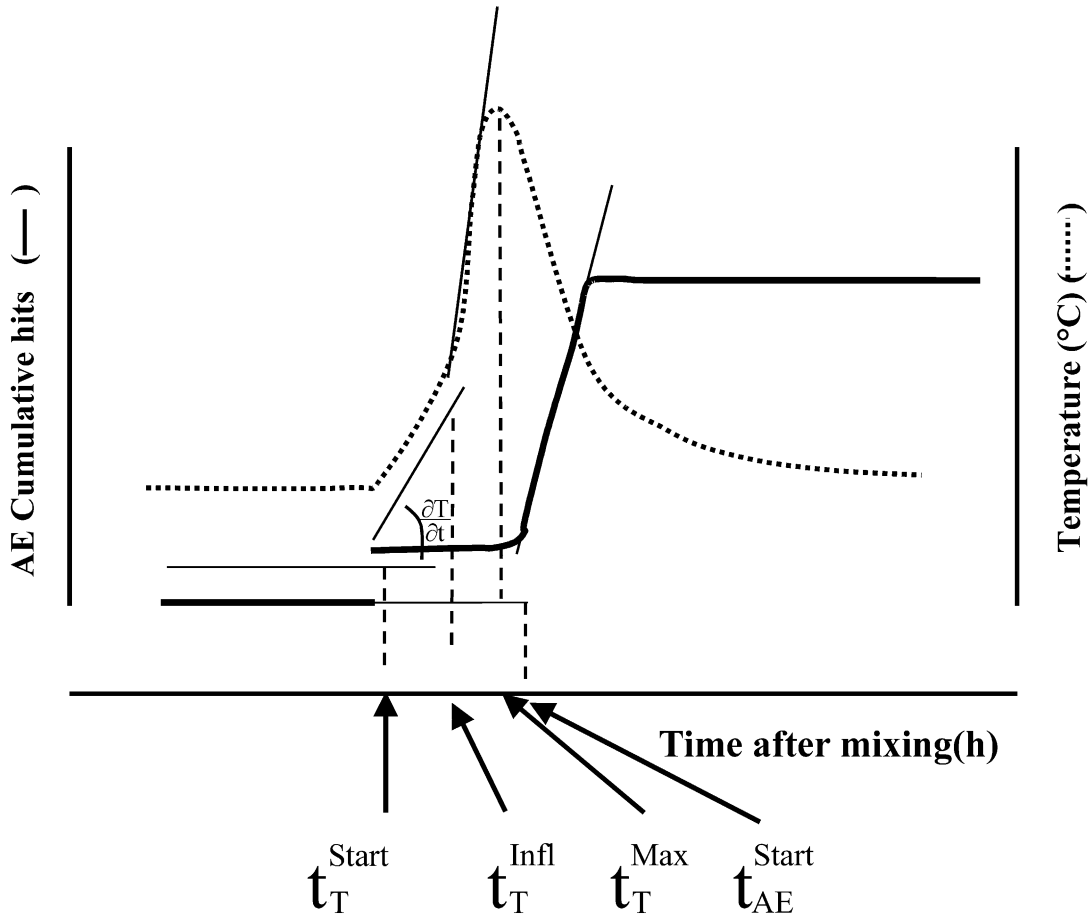

Fig. 6. Schematic representation of AE cumulative number of hits and internal temperature variations as a function of time after mixing. Description of the graphical determination of t_T^{Start}, t_T^{Infl}, t_T^{Max}, t_{AE}^{Start} and $\frac{\partial T}{\partial t}$.

Table 3
Characteristics times and rates for data on Fig. 5

t_T^{Start}	t_{AE}^{Start}	t_T^{Infl}	t_T^{Max}	$\frac{\partial T}{\partial t}$ before the inflexion (α)	$\frac{\partial T}{\partial t}$ after the inflexion (β)
2 h	2.67 h	3.07 h	3.70 h	13 °C/h	24 °C/h

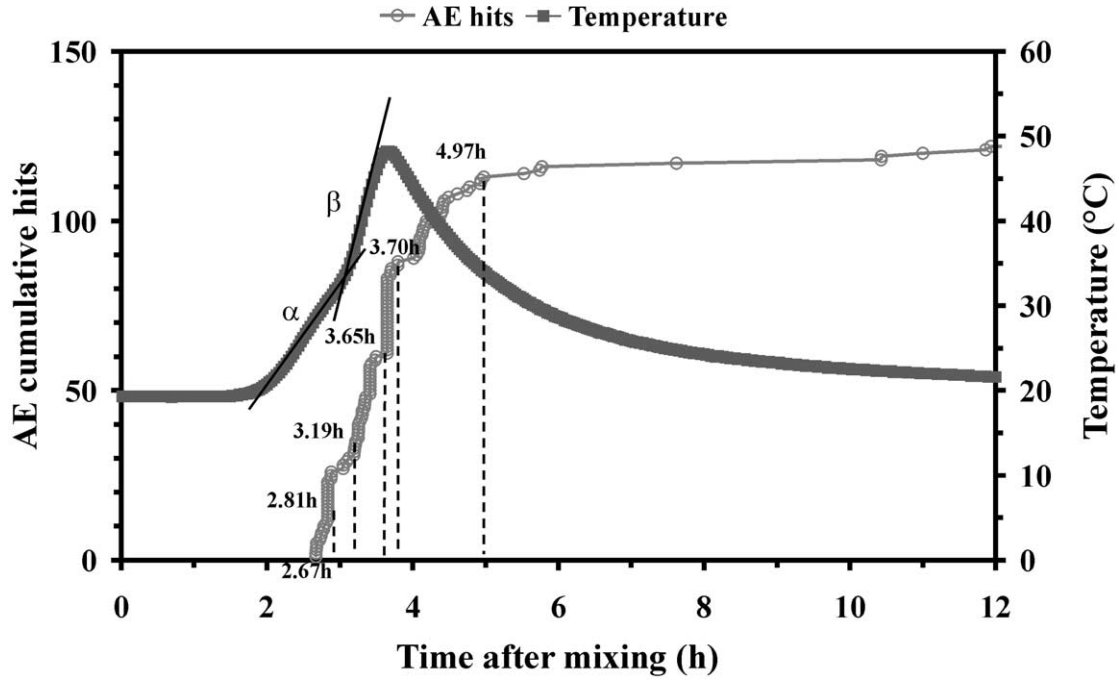

Fig. 7. AE cumulative number of hits and internal temperature as a function of time after mixing. Magnification of Fig. 5 for the first 12 h.

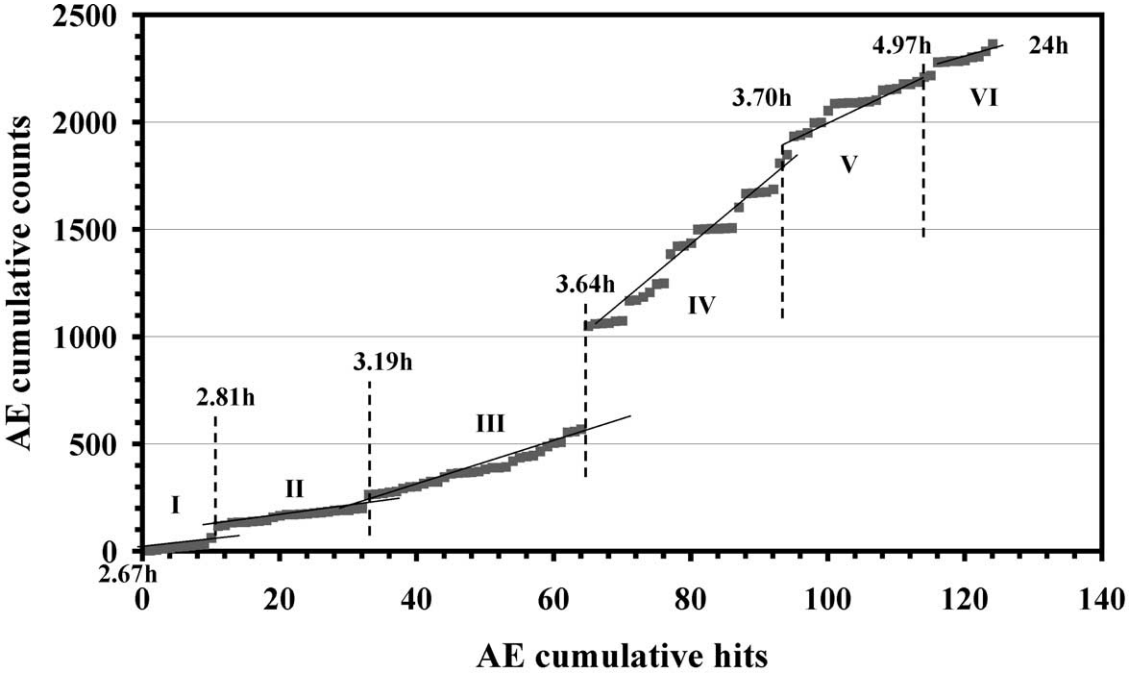

Fig. 8. AE cumulative number of counts as a function of AE cumulative number of hits. Identification of the different AE periods.

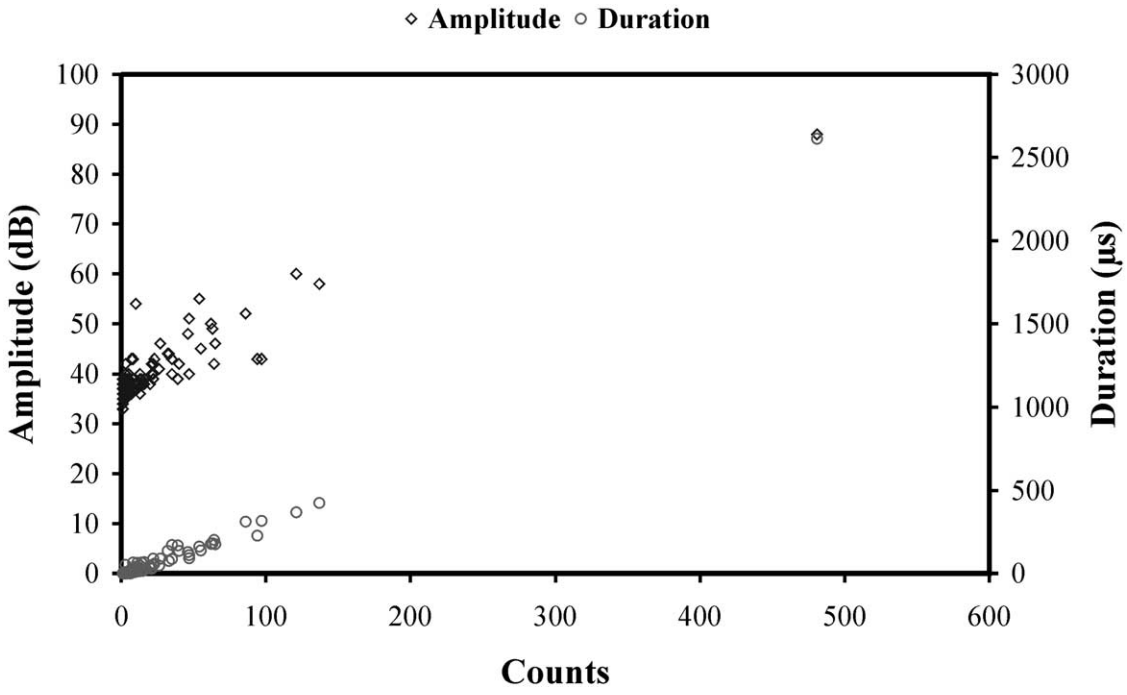

Fig. 9. Typical evolution of amplitude and duration of hits as a function of counts during AE testing of a cement specimen.

beginning of the massive hydrate precipitation. This process has already been studied by AE technique[36] and the authors concluded that it could generate acoustic activity induced by contact interactions between the particles. This can explain the low values of the associated average number of counts per hit which illustrate a low energy phenomenon.

During the next two periods ((III): 3.19–3.65 h, (IV): 3.65–3.70 h), a rise of the AE features (hit rate, average number of counts per hit) is observed (i.e. Table 4). During these periods, the massive precipitation of hydration products continues and the material begins to stiffen. At this time, a growth of crystalline phases is observed and the rigidity of the material is due to the tangling of hydrates (Fig. 10). This process can produce a high AE activity associated with the high-energy rubbing between the hydrates. For these two periods, and especially for period IV, the hit rate and the average number of counts per hit reach their maximum values, 460 h^{-1} and 34.2, respectively. This result is in accordance with the previous discussion.

If we analyse precisely the AE features during period V, we notice a strong reduction (92%) of the hit rate (460 to 36 h^{-1}) associated to a smaller one (29%) for the average number of counts per hit (34.2–24.2). It is interesting to remember that the beginning of this period corresponds with t_T^{Max}. If we refer to the above discussion, we observe here that the AE activity is highly reduced, but the energy generated by the phenomenon keeps a reasonable value. The onset and propagation of microcracking is probably the predominant process in this period. The cement skeleton continues to stiffen and microcracking is probably induced by the relaxation of the local stress field in the material.

The last period (VI: 4.97–24 h) exhibits a lower value of AE features (0.58 h^{-1} and 16). At this time, the specimen approaches its final stiffness and phenomena, which can be potentially acoustically active, are less numerous.

It is important to note that the limits between time periods and the associated AE activity are not strict and

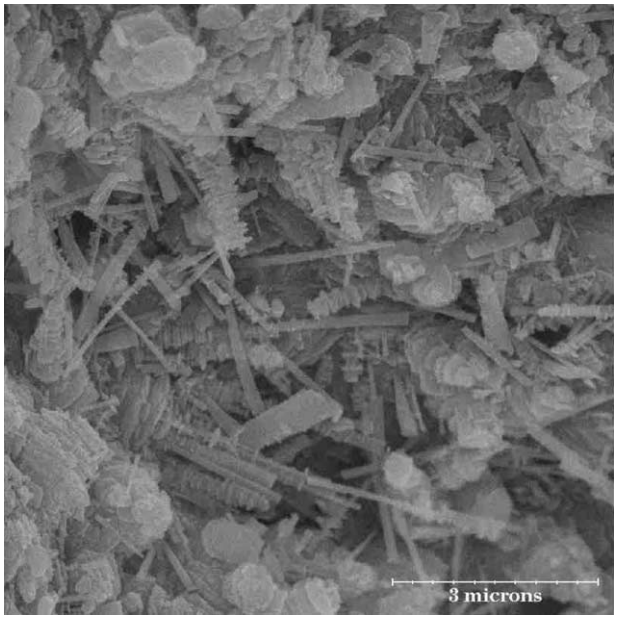

Fig. 10. Scanning electron micrography of hydrated cement specimen. Illustration of tangling of hydrates.

Table 4
Values of AE features for the different time periods

Time period (h)	Number of hits	Time delay (h)	Hit rate (h^{-1})	Average number of counts per hit
0–2.67	0	2.67	0	0
2.67–2.81 (I)	8	0.14	57.1	4.1
2.81–3.19 (II)	23	0.38	60.5	5.1
3.19–3.64 (III)	33	0.45	73.3	9.4
3.64–3.70 (IV)	23	0.05	460	34.2
3.70–4.97 (V)	26	1.33	36.8	24.2
4.97–24 (VI)	11	19.03	0.58	16.1

an overlapping of the different phenomena during the periods is highly probable. Nevertheless, for each period a single phenomenon can be considered as predominant. Contact between hydrates for period I, emptying of pores for period II,[37] rubbing of hydrates for periods III and IV, microcracking for periods V and VI.

3.2. X-ray tomography

Fig. 11 shows the obtained CT images for slice S2 and for increasing times after mixing. A notable evolution of the greyscale can be pointed out as long as the setting time increases.

From 0 h to approximately 2 h (t_{CT}^{start}) after mixing, the corresponding CT image (Fig. 11a) exhibits a fairly homogeneous level of greyscale which suggests that the density of the tested medium is also relatively homogeneous. A more precise examination of the micrograph shows that a clearer layer can be observed at the bottom of the sample. This specific zone, which corresponds to a localised high-density area, can be probably attributed to an early sedimentation phenomenon due to the difference in density between the water and the anhydrous powder. This period, as already described, can be interpreted as the "dormant period". Therefore, the CT image relates to the simultaneous presence of water and cement.

At 3 h after mixing (Fig. 11b), a dark area appears in the centre of the specimen. This reveals a notable decrease of the absorption of the material. It is important to note that the internal temperature recorded in the sample reaches its highest value (48.1 °C) at approximately the same time ($t_T^{Max} = 3.07$ h). At this temperature, water probably evaporates. The combination of this water evaporation and the chemical reaction taking place in the sample could induce a variation of the X-ray absorption coefficient. Moreover, some rounded patterns are clearly visible on the CT image. This observation could be related to a phenomenon already observed during pure CAC paste hydration,[38] the "nodular setting", where precipitation of hydrates occurs at a few isolated nuclei, forming nodules. Besides, an X-ray absorption gradient is observed between the centre and the edges of the specimen under test. This fact can be due to the heterogeneity of the thermal field which occurs in the material during setting. As already pointed out, the massive formation of hydrates is associated with an exothermic reaction. In our case, the heat diffusion in the material is heterogeneous and can induce gradient in hydrates formation within the volume of the sample. In the heart of the sample, where the temperature is highest, the hydration is more advanced than at the edges.

As the setting time increases, the hydration carries on and a clearing of the corresponding CT image (Fig. 11c) is observed. To summarise, from 2 to 5.75 h after mixing, where massive hydration takes place, the X-ray absorption seems first to decrease (Fig. 11b), and subsequently to increase (Fig. 11c and d). During this period, the material is also stiffening. Beyond this time, the evolution of the greyscale on the CT image is less marked as the setting time increases (comparison between Fig. 11d and e), and the grey seems to be more uniform. The greyscale of the corresponding CT image (Fig. 11e) is slightly darker than the initial one (Fig. 11a). This observation denotes that the final average X-ray absorption of the set cement is lower than in the initial mix (anhydrous cement + water).

In order to discuss and to validate these observations, some quantitative measurements have been performed on several slices at different setting times. The histograms of the corresponding X-ray absorption values deduced from the CT images previously discussed (Fig. 11) are presented in Fig. 12. This graph clearly illustrates what we can call a "boomerang effect" of the average X-ray absorption variation. The initial value is nearby 1650 HU. After 2 h, a drop from 1650 HU to approximately 1300 HU is observed. From 4.5 h, the average X-ray absorption re-increases to reach its final value (1550 HU). Considering this variation of X-ray absorption, a possible explanation could be summarised as follows: crystallised particles in the initial mix (anhydrous powder) keep the average absorption coefficient at its initial value. Then, the massive precipitation of small amorphous germs induces a local variation of the atomic density especially in the centre of the sample where the highest temperature has been recorded. At this time, water evaporates. This variation can affect

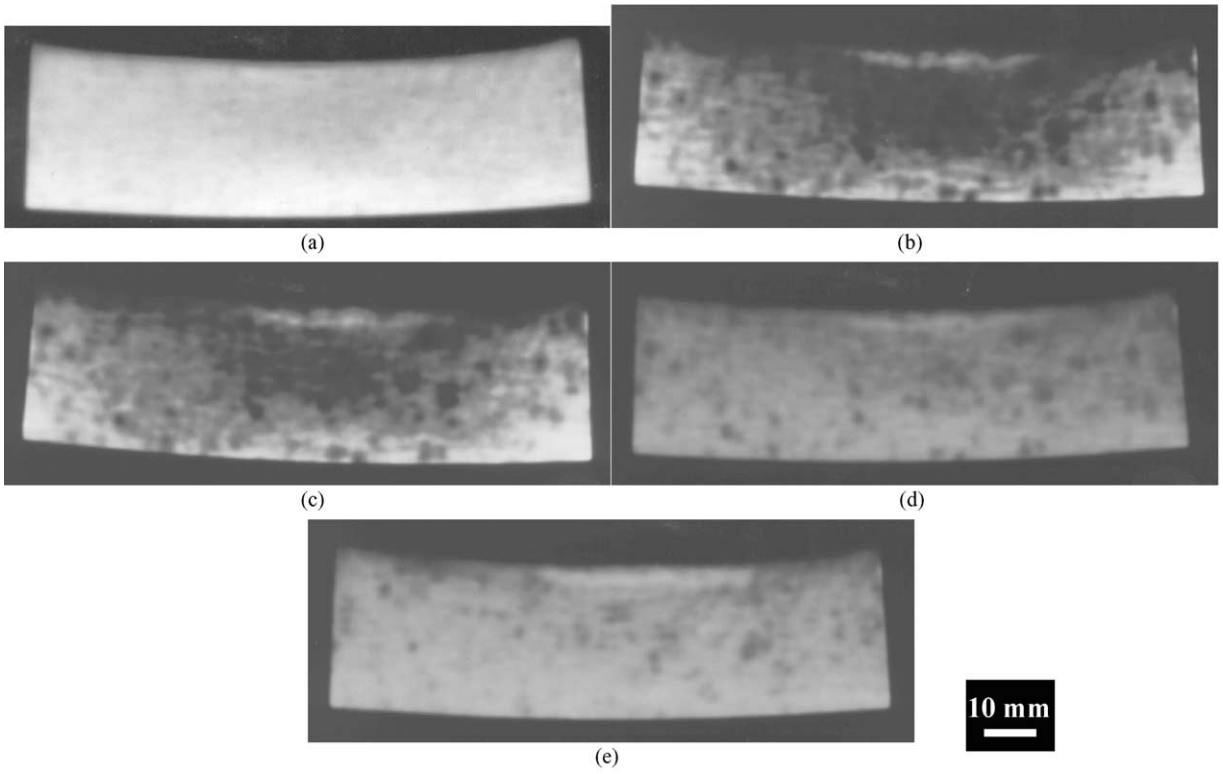

Fig. 11. CT images for S2 slice at different times after mixing: (a) 1 h, (b) 3 h, (c) 4.5 h, (d) 5.75 h, (e) 24 h.

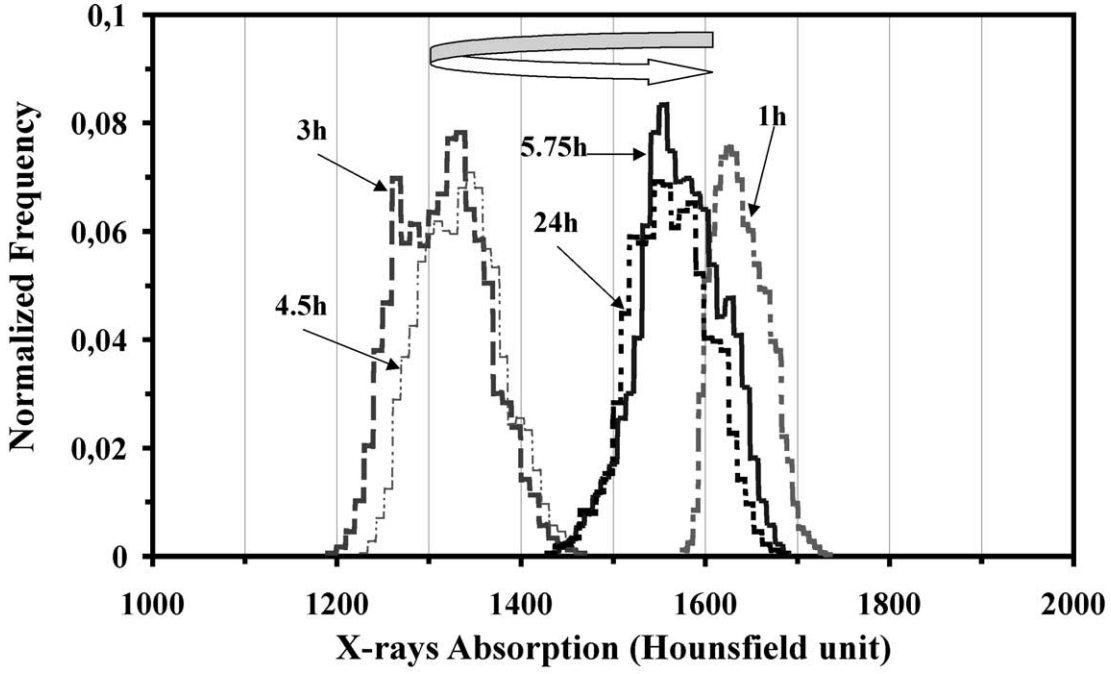

Fig. 12. Histograms of the X-rays absorption for S2 slice (centre) deduced from measurements performed on Fig. 11.

notably the average X-ray absorption of the sample. Afterwards, hydrated phases grow and crystallise; this crystallisation can be responsible for a local variation of the atomic density that affect the value of the absorption coefficient.

If we compare the evolution of the different sets of data, namely qualitative observations, CT measurements such as histograms, ROI and line graphs, we can propose the following chronology, divided into five stages which are pointed out in Fig. 13.

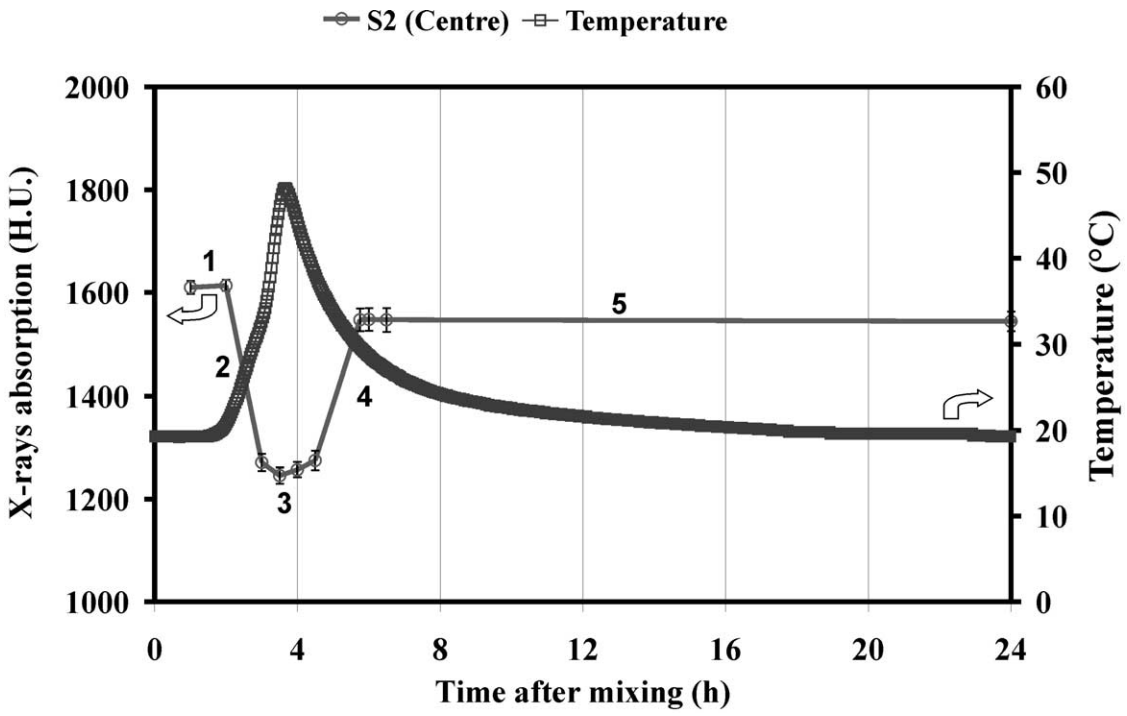

Fig. 13. X-rays absorption and internal temperature measurements as a function of setting time for the S2 slice (centre).

Stage 1 (0–2 h after mixing): the X-ray absorption distribution is relatively homogeneous in the sample. During this first period, hydrates are probably formed in very low amounts.

Stage 2 (2–3 h after mixing): a strong fall of the X-ray absorption value of the specimen is observed. It can be explained by massive production of hydrates and also by evaporation of water.

Stage 3 (3–4.5 h after mixing): slight evolution of X-ray absorption while the hydration continues.

Stage 4 (4.5–5.75 h after mixing): increase of the X-ray absorption of the sample closely related to the crystallisation of hydrates. Beginning of the stiffening of the specimen.

Stage 5 (5.75–24 h after mixing): the sample reaches its final state.

4. Conclusion

This paper describes the monitoring of the early hydration of Secar71 cement paste (W/C = 0.33) by both acoustic emission (AE) and X-ray computed tomography (CT) techniques Qualitative observations and quantitative measurements make it possible to propose some concluding remarks:

- The AE and CT techniques can usefully describe the early hydration of a cement paste either in terms of the chronology of mechanisms (AE) or changes in the atomic arrangement of the material (CT).
- The ranges of investigation of these two techniques are complementary. CT gives information on the evolution of the material at the microscopic scale (nucleation) concerning chemical effects. The AE technique makes it possible to follow the phenomena at mesoscopic (rubbing of hydrates, cracking onset) and macroscopic (cracking propagation) scales, describing the induced mechanical effects.
- CT can reveal the location in the sample of a phenomenon which is identified by AE.
- The comparison between the different results obtained by AE, CT or temperature measurements shows that there is some close correlation. If we compare it with the internal temperature data, then the CT technique seems to be more sensitive to the dissolution-nucleation process (no time delay observed between t_{CT}^{start} and t_{T}^{start}) than the AE technique. Moreover, a good correspondence in time (number of periods, time start) has been observed.

Lastly, the important advantage of these non-destructive, in situ and real time techniques, is that they can be applied to fairly large specimens (cement, mortars or concrete). This study shows, one more time, that the power of characterisation science can be easily enhanced by a the appropriate combination of complementary techniques.

References

1. Midgley, H. G.. In *Calcium Aluminate Cements*, ed. R. J. Mangabhai. Chapman and Hall, London, 1990, pp. 1–13.
2. Scrivener, K.L., Historical and present day applications of calcium aluminate cements. In *Calcium Aluminate Cements 2001*, ed. R.J. Mangabhai and F.P. Glasser. 2001, pp. 3–23.
3. Gessner, W., Recent researches on calcium aluminate hydration. In *Calcium Aluminate Cements 2001*, ed. R.J. Mangabhai and F.P. Glasser. 2001, pp. 151–154.
4. Capmas, A., Ménétrier-Sorrentino, D., and Damidot, D., Effect of temperature on setting time of calcium aluminate cements. In *Calcium Aluminate Cements*, ed. R. J. Mangabhai, and E. F. Spon. 1990.
5. Fujii, K., Kondo, W. and Ueno, H., Kinetics of hydration of monocalcium aluminate. *J. Am. Ceram. Soc.*, 1986, **69**(4), 361–364.
6. Edmonds, R. N. and Majumdar, A. J., The hydration of monocalcium aluminate at different temperatures. *Cem. Conc. Res.*, 1988, **18**(2), 311–320.
7. Barnes, P., Clark, S. M., Hausermann, D., Henderson, E., Fentiman, C. H., Muhamad, M. N. and Rashid, S., Time-resolved studies of the early hydration of cements using synchrotron energy-dispersive diffraction. *Phase Transitions*, 1992, **39**, 117–128.
8. Chatterjiand, S. and Majumdar, A. J., Studies of the early stages of paste hydration of high alumina cements. I: Hydration of individual aluminate. *Ind. Concr. Jour*, 1966, 51–55.
9. Richard, N., *Structure et Propriétés Élastiques des Phases Cimentières de Mono-aluminate de Calcium*. PhD thesis, Paris VI University, France, 1996.
10. Cong, X. and Kirkpatrick, R. J., Hydration of calcium aluminate cements: a solid-state ^{27}Al NMR study. *J. Am. Ceram. Soc.*, 1993, **76**(2), 409–416.
11. Rashid, S., Barnes, P., Bensted, J. and Turrilas, X., Conversion of calcium aluminate cement hydrates re-examined with synchrotron energy-dispersive diffraction. *J. Mater. Sci. Lett.*, 1994, **13**, 1232–1234.
12. Rashid, S. and Turrillas, X., Hydration kinetics of $CaAl_2O_4$ using synchrotron energy-dispersive diffraction. *Thermochim. Acta*, 1997, **302**, 25–34.
13. Monteiro, P. J. M. and King, M. S., Experimental studies of elastic wave propagation in high-strength mortar. *Am. Cer. Soc. Test. Mater.*, 1998, 68–74.
14. Harker, A. H., Schofield, P., Stimpson, B. P., Taylor, R. G. and Temple, J. A. G., Ultrasonic propagation in slurries. *Ultrasonics*, 1991, **29**, 427–438.
15. Cutard, T., Fargeot, D., Gault, C. and Huger, M., Time delay and phase shift measurement for ultrasonic pulses using autocorrelation methods. *J. Appl. Phys.*, 1994, **75**, 1909–1913.
16. Öztürk, T., Rapoport, J., Popovics, J. S. and Shah, S. P., Monitoring the setting and hardening of cement-based materials with ultrasound. *Conc. Sc. Eng.*, 1999, **1**, 83–91.
17. Sayers, C. M. and Grenfell, R. L., Ultrasonic propagation through hydrating cement. *Ultrasonics*, 1993, **31**, 147–153.
18. Sayers, C. M. and Dahlin, A., Propagation of ultrasound through hydrating cement pastes at early times. *Adv. Cem. Bas. Mater.*, 1993, **1**, 12–21.
19. Mayfield, B. and Bettison, M., Ultrasonic pulse testing of high alumina cement concrete. *Concrete*, 1974, 36–38.
20. Boumiz, A., Vernet, C. and Cohen-Tenoudji, F., Mechanical properties of cement and mortars at early ages. *Adv. Cem. Bas. Mater.*, 1996, **1**, 94–106.
21. Chotard, T., Gimet-Bréart, N., Smith, A., Fargeot, D., Bonnet, J. P. and Gault, C., Application of ultrasonic testing to describe the hydration of calcium aluminate cement at the early age. *Cem. Concr. Res.*, 2001, **31**, 405–412.
22. Barré, S. and Benzeggagh, M. L., On the use of acoustic emission to investigate damage mechanisms in glass-fibre-reinforced polypropylene. *Comp. Sci. Technol.*, 1994, **52**, 369–376.
23. Havlicek, F. and Crha, J., Acoustic emission monitoring during solidification processes. *J. Acous. Emi.*, 1999, **17**, 3–4.
24. Coddet, C., Chretien, J. F. and Beranger, G., Investigation on the fracture mechanism of oxide layers growing on titanium by acoustic emission. *Titanium and Titanium Alloys: Scientific and Technological Aspects*, 1982, **2**, 1097–1105.
25. Phillips, D. H. and Lannutti, J. J., X-ray computed tomography for the testing and evaluation of ceramic processes. *Am. Cer. Soc. Bull.*, 1992, **71**, 1410–1416.
26. Phillips, D. H. and Lannutti, J. J., Measuring physical density with X-ray computed tomography. *NDT Int.*, 1997, **30**, 339–350.
27. Smith, A., Chotard, T., Gimet-Breart, N. and Fargeot, D., Correlation between hydration mechanism and ultrasonic measurements in an aluminous cement: effect of setting time and temperature on the early hydration. *J. Eur. Ceram. Soc.*, 2002, **22**, 1947–1958.
28. Prosser, W. H., Jackson, K. E., Kellas, S., Smith, B. T., McKeon, J. and Friedman, A., Advanced waveform-based acoustic emission detection of matrix cracking in composites. *Mater. Eval.*, 1995, 1052–1058.
29. Suzuki, H., Takemoto, M. and Ono, K., The fracture dynamics in a dissipative glass fibber/epoxy model composite with AE source simulation analysis. *J. Acous. Emis.*, 1996, **14**, 35–50.
30. Bakuckas, J. G., Prosser, W. H. and Johnson, W. S., Monitoring damage growth in titanium matrix composites using acoustic emission. *J. Comp. Mater.*, 1994, **28**, 305–328.
31. Berkovits, A. and Fang, D., Study of fatigue crack characteristics by acoustic emission. *Eng. Fract. Mech.*, 1995, **51**, 401–416.
32. Ohtsu, M., Tomoda, Y. and Fujioka, T., *Estimation of Initial Damage in Concrete by Acoustic Emission*. 1997, Fourth Far East Conference on NDT.
33. Uomoto, T., Application of acoustic emission to the field of concrete engineering. *J. Acous. Emis.*, 1987, **6**, 137–144.
34. Deis, T. A. and Lannutti, J. J., X-ray computed tomography for evaluation of density gradient formation during the compaction of spray-dried granules. *J. Am. Ceram. Soc.*, 1998, **81**, 1237–1247.
35. Wu, K., Chen, B. and Yao, W., Study on the AE characteristics of fracture process of mortar, concrete and steel-fibre-reinforced concrete beams. *Cem. Conc. Res.*, 2000, **30**, 1495–1500.
36. Chotard, T., Smith, A., Codet, N., de Bailliencourt, M., Fargeot, D. and Gault, C., New applications of acoustic emission technique for real-time monitoring of material processes. *J. Mater. Sci. Lett.* 2002 (in press).
37. Chotard, T., Smith, A., Rotureau, D., Fargeot, D. and Gault, C., Acoustic emission characterisation of calcium aluminate cement hydration at an early stage. *J. Eur. Ceram. Soc.*, 2003, **23**, 387–398.
38. Lamour, V. R. H., Monteiro, P. J. M., Scrivener, K. L. and Fryda, H., Microscopic studies of the early hydration of calcium aluminate cements. In *Calcium Aluminate Cements 2001*, ed. R. J. Mangabhai and F. P. Glasser. IOM communications, London, 2001, pp. 169–180.